An Evaluation of Measured Pressure Signatures From Wind-Tunnel Models of Three Low-Boom Concepts

Robert J. Mack
Langley Research Center, Hampton, Virginia

Since its founding, NASA has been dedicated to the advancement of aeronautics and space science. The NASA Scientific and Technical Information (STI) Program Office plays a key part in helping NASA maintain this important role.

The NASA STI Program Office is operated by Langley Research Center, the lead center for NASA's scientific and technical information. The NASA STI Program Office provides access to the NASA STI Database, the largest collection of aeronautical and space science STI in the world. The Program Office is also NASA's institutional mechanism for disseminating the results of its research and development activities. These results are published by NASA in the NASA STI Report Series, which includes the following report types:

- TECHNICAL PUBLICATION. Reports of completed research or a major significant phase of research that present the results of NASA programs and include extensive data or theoretical analysis. Includes compilations of significant scientific and technical data and information deemed to be of continuing reference value. NASA counterpart of peer-reviewed formal professional papers, but having less stringent limitations on manuscript length and extent of graphic presentations.

- TECHNICAL MEMORANDUM. Scientific and technical findings that are preliminary or of specialized interest, e.g., quick release reports, working papers, and bibliographies that contain minimal annotation. Does not contain extensive analysis.

- CONTRACTOR REPORT. Scientific and technical findings by NASA-sponsored contractors and grantees.

- CONFERENCE PUBLICATION. Collected papers from scientific and technical conferences, symposia, seminars, or other meetings sponsored or co-sponsored by NASA.

- SPECIAL PUBLICATION. Scientific, technical, or historical information from NASA programs, projects, and missions, often concerned with subjects having substantial public interest.

- TECHNICAL TRANSLATION. English-language translations of foreign scientific and technical material pertinent to NASA's mission.

Specialized services that complement the STI Program Office's diverse offerings include creating custom thesauri, building customized databases, organizing and publishing research results ... even providing videos.

For more information about the NASA STI Program Office, see the following:

- Access the NASA STI Program Home Page at *http://www.sti.nasa.gov*

- E-mail your question via the Internet to help@sti.nasa.gov

- Fax your question to the NASA STI Help Desk at (301) 621-0134

- Phone the NASA STI Help Desk at (301) 621-0390

- Write to:
  NASA STI Help Desk
  NASA Center for AeroSpace Information
  7121 Standard Drive
  Hanover, MD 21076-1320

An Evaluation of Measured Pressure Signatures From Wind-Tunnel Models of Three Low-Boom Concepts

Robert J. Mack
Langley Research Center, Hampton, Virginia

December 2005

Available from:

Summary

Existing sonic-boom design and analysis methodology was revised and modified as the result of a low-boom method validation study done during the years 1990-1991. Then, three low-boom concepts were designed with this revised methodology to assess its applicability and validity. Models of these concepts were built, and used to measure pressure signatures in the wind tunnel. An analysis of this wind-tunnel data showed unexpected nacelle-inlet and the nacelle-wing interference-lift shocks in the pressure signatures from the two models with engines under the wings, but not in the pressure signatures from the wind-tunnel model with the engine nacelles mounted on the aft fuselage. However, additional lift-induced shocks were found in the pressure signature data from all three wind-tunnel models indicating that other lift-induced effects were present.

Introduction

Supersonic-cruise conceptual and real aircraft have been designed with components integrated to maximize aerodynamic efficiency, while minimizing empty weight. Engine nacelles are usually mounted under the wings; the location seen on the United States' XB-70, the English-French Concorde, and the Russian Tu-144, references 1 to 3. This engine-nacelle location increased aerodynamic efficiency by generating favorable nacelle-wing interference lift (reduced drag-due-to-lift from the wing), enhanced propulsion efficiency by placing the engine inlets in a reduced Mach number flow field, aided structural efficiency by positioning the engines and nacelles near major wing spars, and helped with the balancing of the aircraft by having the engines close to the configuration's fuel tanks and center of gravity. Most of the conceptual High-Speed Civil Transport (HSCT) aircraft studied in more recent years followed this conventional engines-under-the-wing design strategy. References 4 through 10 documented configurations designed during the United States' Supersonic Transport (SST) Program and the follow-on Supersonic Cruise Aircraft Research (SCAR) Program studies of design, propulsion, cost, and marketing problems.

Research into the technical and operational problems of a commercial supersonic-cruise aircraft was resumed with the start of the High Speed Research (HSR) program. Existing sonic-boom design and analysis methods were employed to design two theory-validation concepts, reference 11, with the engine nacelles in the usual under-the-wing location. Wind-tunnel models were built, and pressure signatures were measured. An analysis of the measured pressure signatures revealed unexpected nacelle-inlet and nacelle-wing interference-lift shocks. These conclusions lead to a revision of existing low-boom design strategies, nacelle integration techniques, and sonic-boom analysis methods.

Three low-boom conceptual HSCT aircraft were then designed with the modified methods to evaluate, and hopefully validate, their capabilities. Two of these concepts had nacelles in the conventional under-the-wing location. The third concept had the engine nacelles mounted on the aft fuselage, behind the wing trailing edge, so there would be no nacelle-wing interference-lift pressure disturbances in the flow field.

In this paper, the wind-tunnel data that lead to the modification of 1970's low-boom design ideas, sonic-boom analysis methods, and nacelle-integration techniques are presented and discussed. The three follow-on HSCT concepts designed with these modified sonic-boom analysis methods and low-boom design strategies are also described and discussed. Samples of measured pressure signatures from wind-tunnel models of these three follow-on concepts are presented and analyzed so that the merits of the different design strategies can be assessed. The results of this analysis are used to judge the capabilities of the design methods, and the effectiveness of the nacelle-integration techniques.

Nomenclature

A_E	equivalent area, ft^2
b	wing span, ft
C_L	lift coefficient
$C_{L,CRUISE}$	lift coefficient at supersonic-cruise conditions
$F(y)$	Whitham F-function of variable y, $\text{ft}^{1/2}$
h	cruise altitude or separation distance, ft or in
I	maximum value of $\int \frac{\Delta p}{p} dx$
M	Mach number
p	ambient pressure, psf
Δp	overpressure, psf
S	wing area, ft^2
W_{BC}	beginning cruise weight, lb
W_E	concept empty weight, lb
W_{GTO}	aircraft gross takeoff weight, lb
y	Whitham F-function variable, ft

Reasons For Modification Of Sonic-Boom Methodology

Review Of Existing Methods

At the start of the HSR program, the existing methodology for analyzing and designing low-boom concepts, and integrating nacelles, was tested by measuring pressure signatures generated by wind-tunnel models of Mach 2 and Mach 3 theory-validation concepts, reference 11. The configurations of the two concepts had been low-boom tailored to produce a 1.0 psf ground overpressure with design and analysis methodology developed and described in references 12 and 13. Sketches of these concepts are shown in figure 1 and 2.
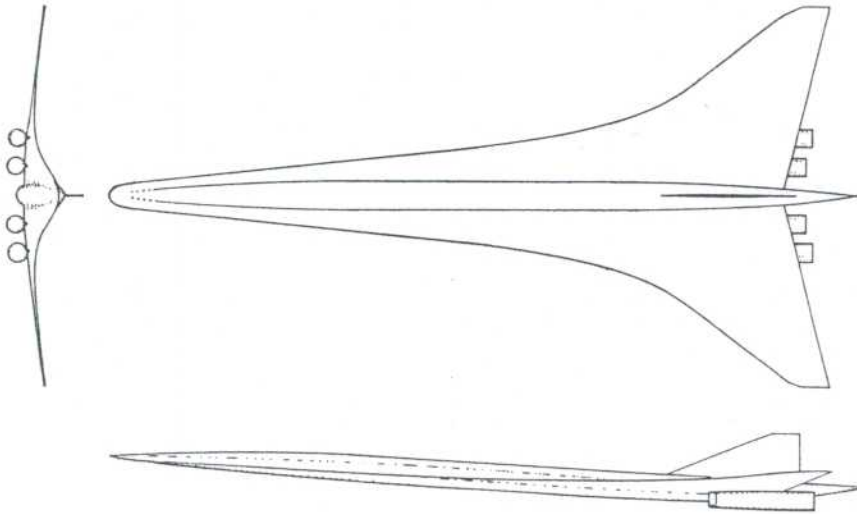
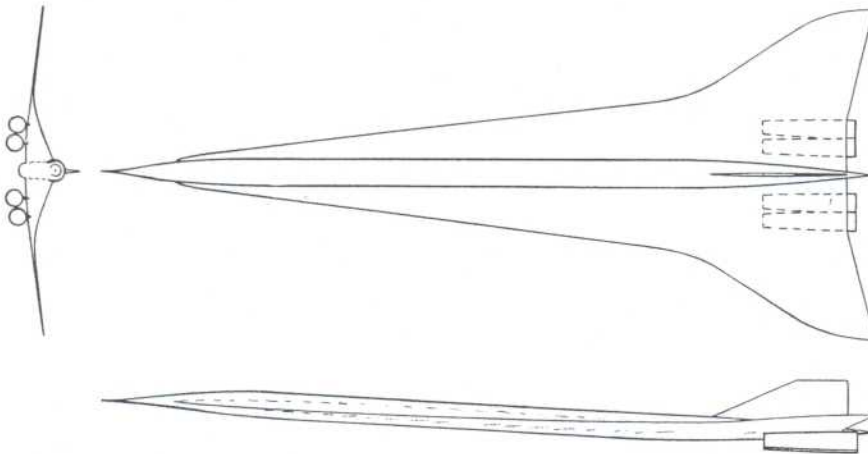Figure 1. Three view of the Mach 2 low-boom theory-validation concept.

Figure 2. Three view of the Mach 3 low-boom theory-validation concept.

During the measurement of pressure signatures from both the Mach 2 and the Mach 3 models, unexpected shocks were observed between the nose shock and the expansion to the tail shock. These unexpected shocks can be seen in the pressure signatures shown in figures 3 and 4.
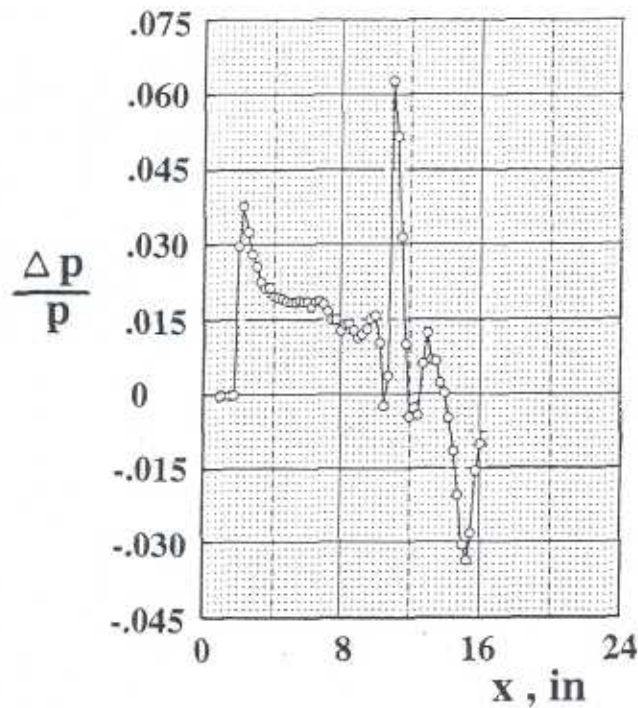
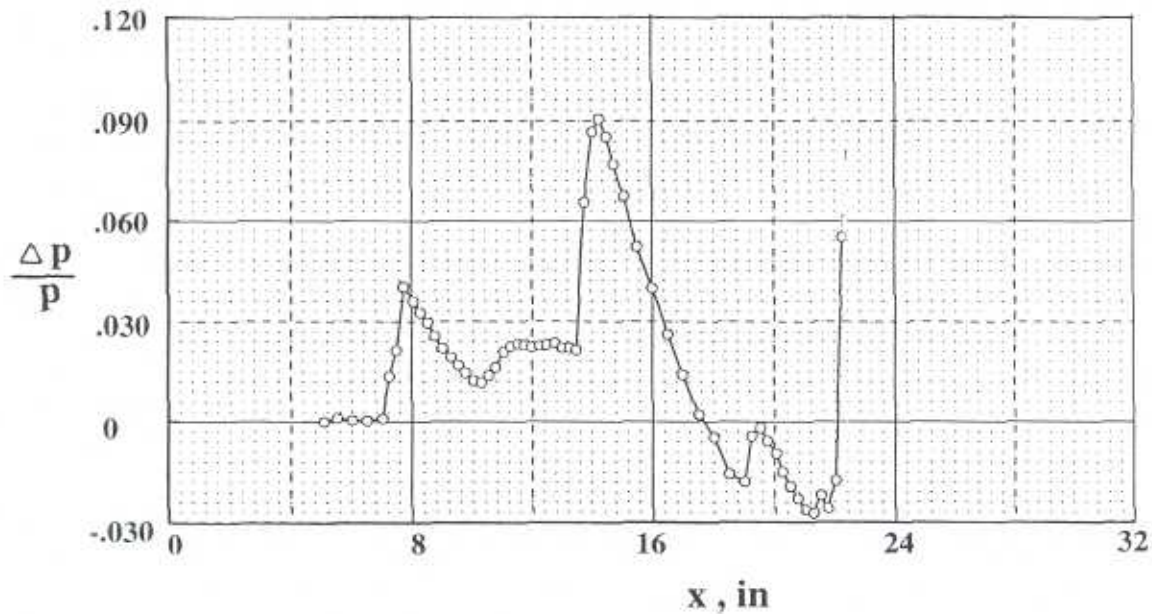Figure 3. Mach 2 model pressure signature. Nacelles on, M = 2.0, h = 6 in, C_L = 0.0680.

Figure 4. Mach 3 model pressure signature. Nacelles on, M = 2.96, h = 8.5 in, C_L = 0.0545.

   The Mach 2 and Mach 3 models were the first sonic-boom models large enough to have flow-through ducted nacelles. Since such shocks had not been seen before, these nacelles were suspected of being the cause. To test this hypothesis, pressure signatures from models, without nacelles, were measured. The pressure signature from the Mach 2 model is shown in figure 5,
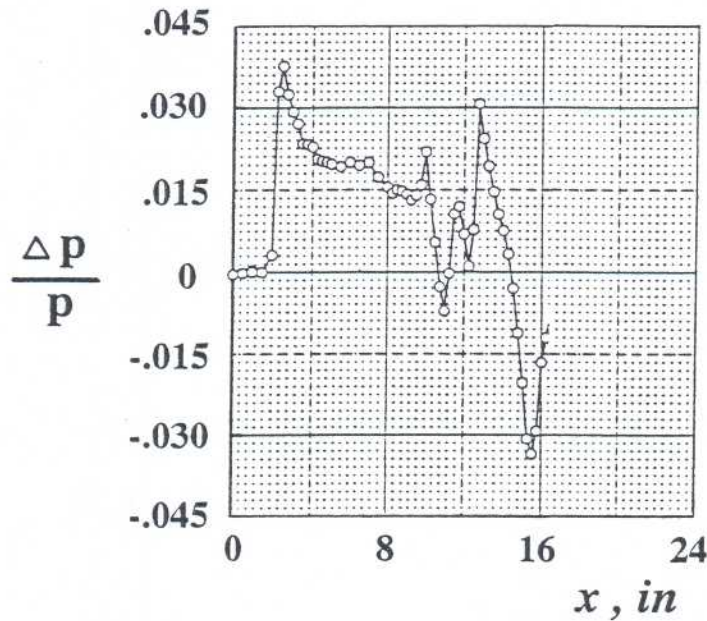
Figure 5. Mach 2 model pressure signature. Nacelles off, M = 2.0, h = 6 in, C_L = 0.0680.

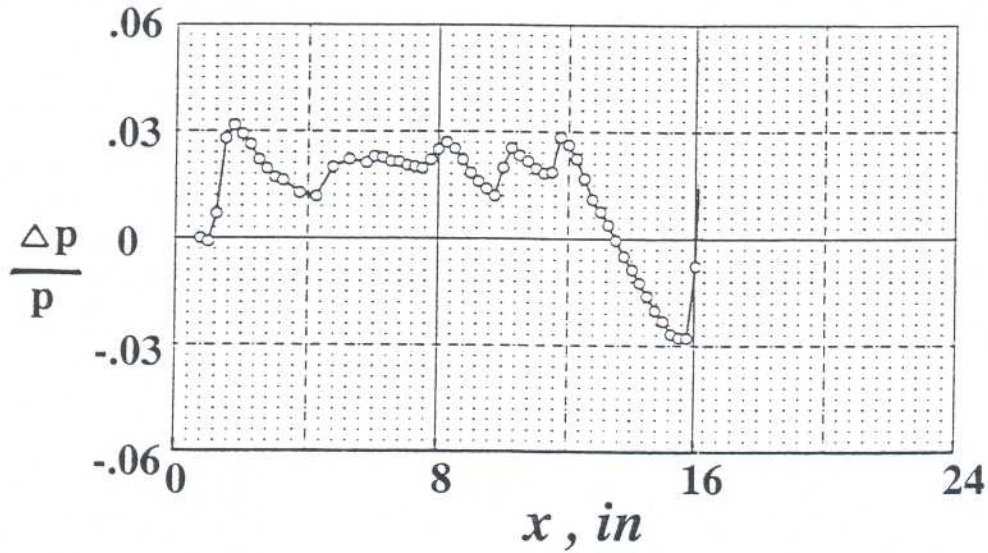and the pressure signature from the Mach 3 model is shown in figure 6.

Figure 6. Mach 3 model pressure signatures. Nacelles off, M = 2.96, h = 8.5 in, C_L = 0.0545.

When figure 3 is compared with figure 5, and figure 4 with figure 6, the strong shocks caused by the presence and the location of the engine nacelles is readily seen and identified. The appearance of these shocks was not initially understood, since both models had been configured and low-boom tailored with the latest low-boom design methods. So, the first step was an evaluation of the methodology used for sonic-boom analysis, low-boom design, and nacelle integration.

Evaluation Of Initial Methods

Design and analysis methods in use before the HSR program were based on slender-body theory assumptions. The first assumption was that the engine nacelles, like other small-disturbance bodies, had smooth-and-continuous surface slopes. Since the aerodynamic volume of the nacelle (integral of the cross-section area minus the inlet area along the length) was small, and the area growth was similar to that of the fuselage and wing volumes, it seemed reasonable to assume that the nacelle equivalent areas contributed little to the net equivalent areas of the aircraft. The far-field Whitham F-function, reference 14, calculated from these summed equivalent areas and used to obtain ground overpressures, was also had this assumption.

However, these assumptions were not met on all the components of HSCT concepts or their wind-tunnel models. It was noted that the Whitham F-function of the engine nacelle started with a finite discontinuity, $F(0) > 0$, *because of a finite nacelle inlet radius and a non-zero inlet-lip angle, i.e. a radius discontinuity.* These two factors, a non-zero inlet diameter and a finite lip angle, meant that engine nacelles could not be physically treated like conventional small-disturbance components. Instead, each nacelle F-function had to be calculated separately, and then added to the wing/fuselage/fin(s) F-function to obtain a summed F-function for the aircraft.

The second assumption was the growth of the nacelle-wing interference-lift equivalent areas was also smooth and continuous. Actually, the nacelle-wing interference-lift equivalent areas had a linear gradient at their origin. So, the nacelle-wing interference-lift F-function also began with a discontinuity, $F(0) > 0$, and it's sonic-boom analytical treatment had to be similar to that given the ducted engine nacelle volume.

This methodology re-evaluation was presented in reference 15, where it was shown that: (1) sharp lip-angle ducted nacelles could generate flow-field shocks whether the nacelles were positioned by either low-drag or low-boom criteria, and under both choked-flow and unchoked-flow conditions; and (2) the equivalent area distribution of the nacelle-wing interference lift produced a Whitham F-function with a singularity at its start like the Whitham F-function of a ducted nacelle. This re-evaluation resulted in a significant revision of existing sonic-boom analyses, nacelle integration techniques, and low-boom design methods.

Revisions To Initial Methods

Existing low-boom design and sonic-boom analysis methods could be used if a few minor modifications were made to the mathematical treatment of the aircraft's components. First, component equivalent areas could be summed *if, and only if,* each component's equivalent area distribution was smooth and continuous. Second, the F-functions of components like engine nacelles, supersonic leading edge canards, and supersonic leading edge horizontal tails had to be calculated separately. They were then combined with the F-functions from components with smooth and continuous equivalent area distributions, to obtain a summed F-function which would represent the sonic-boom disturbance function of the entire aircraft. This summation of component F-functions would be the basis for the prediction of the ground pressure signatures for a specified cruise Mach number, beginning-cruise altitude, and beginning-cruise weight. In this manner, the revised methodology had most of the previous design method's simplicity and flexibility, and retained all the accuracy of the original Whitham theory, reference 14.

Application Of Revised Method

Follow-on Low-Boom Concepts

Although the revised methods for predicting sonic-boom overpressures, designing low-boom concepts, and integrating engine nacelles seemed physically and mathematically correct, they needed to be validated. The first step toward validation was to design new low-boom concepts with these revised methods. An assessment of the performance of these concepts would determine whether the mission requirements and the low-boom constraint (1.0 psf overpressure on the ground) could be met with conceptual aircraft similar to the Boeing and the McDonnell Douglas baseline concepts in size, shape, and gross takeoff weight. Mission characteristics would be determined with component weights estimated from the Flight Optimization System (FLOPS) code, reference 16. Sonic-boom overpressure characteristics would be predicted with Whitham theory, and with Computational Fluid Dynamic (CFD) codes coupled with the Thomas pressure signature extrapolation code, reference 17.

Three low-boom concepts were designed for this validation exercise: the B935, the LB-16, and the HSCT-10B, a.k.a. LB-18. Two of the low-boom concepts, the B935 and the LB-16, were designed with the engine nacelles in the conventional under-the-wing location. The third concept, the HSCT-10B, had the engine nacelles mounted on the aft fuselage, well behind the trailing edge of the wing.

The B935
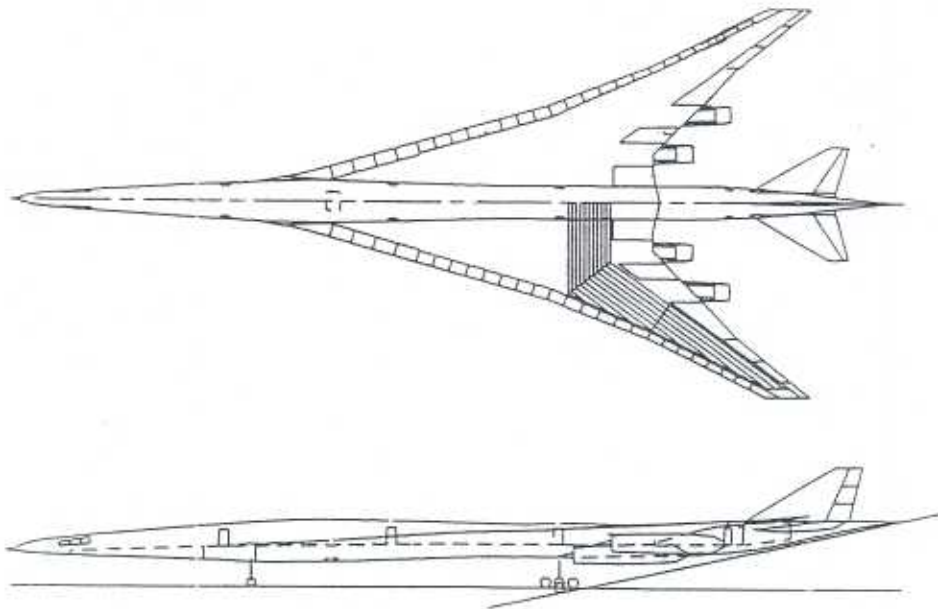The B935, reference 18, low-boom concept is shown in figure 7.

Figure 7. The Boeing B935 conceptual aircraft.

This concept was designed with low-boom tailoring for over-land cruise at Mach 1.7, and would cruise at Mach 2.4 during flight over water.

8

The LB-16
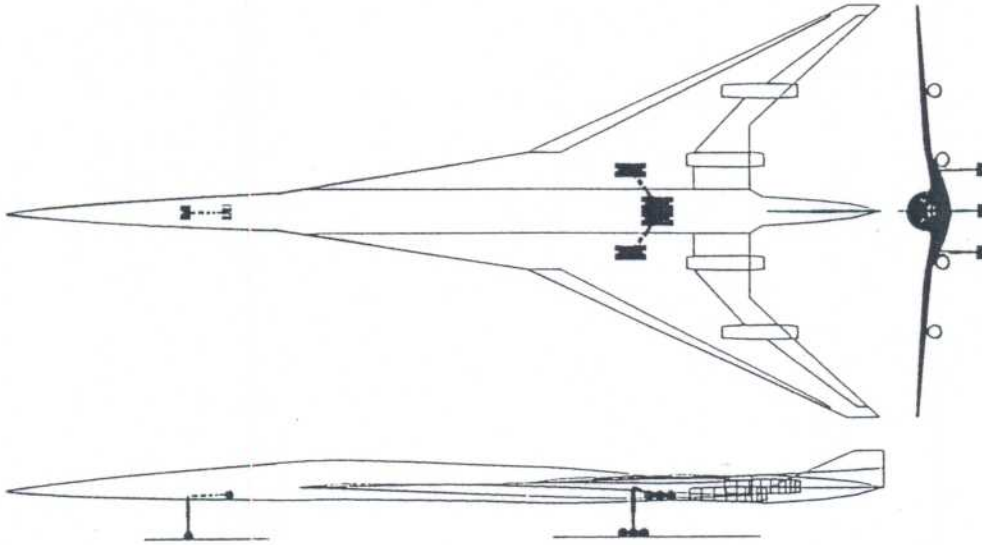The LB-16 low-boom concept, reference 19, is shown in figure 8.

Figure 8. The Langley LB-16 conceptual aircraft.

The LB-16 was designed with low-boom tailoring for over-land cruise at Mach 1.6, and would cruise at Mach 2.0, rather than Mach 2.4, during flight over water.

The HSCT-10B
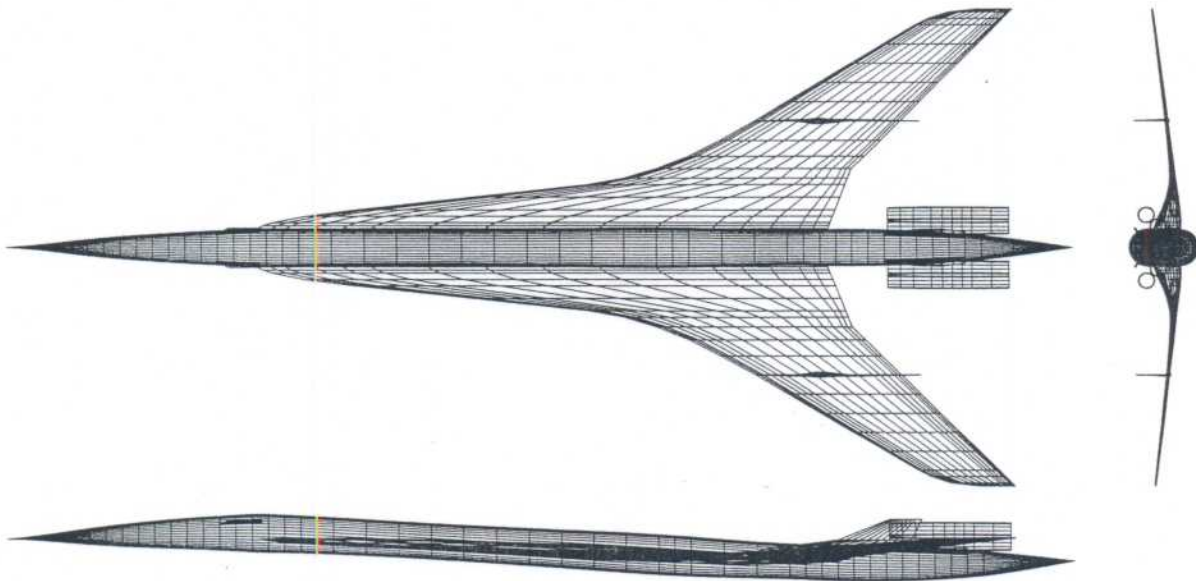The HSCT-10B concept, reference 20, is shown in figure 9.

Figure 9. Computer drawing of the Langley HSCT-10B conceptual aircraft.

This concept was designed with low-boom tailoring for over-land cruise at Mach 1.8, and like the B935 concept, would cruise at Mach 2.4 over water.

In addition to being a low-boom concept, the HSCT-10B concept also served as a reference in this assessment of the merits of the revised nacelle-integration methodology. Its nacelles were on the aft fuselage behind the wing trailing edge, so the nacelle flow-field disturbances would be due to nacelle volume alone. Two sets of nacelles were designed to determine differences in the disturbances from nacelles located at such a rearward position. These sets - one set of small nacelles and one set of large nacelles - were designed for engines with the same thrust level, but different propulsion technology assumptions. The flow-field disturbances generated by either of the nacelle sets would be readily seen in the measured pressure signatures - see figures 3 and 5 or figures 4 and 6 - if the revised nacelle-integration method was inadequate or was improperly applied. Such data would be helpful if the other two models, the B935 and the LB-16, generated pressure signatures with features not readily identified and/or not be unambiguously interpreted.

The designs of these three follow-on low-boom concepts were influenced, to varying degrees, by the Mach 2 and Mach 3 models' wind-tunnel test results. However, each configuration was the result of a slightly different mix of design choices that incorporated varying levels of aerodynamic efficiency, low sonic-boom technology, structural efficiency, and materials technology. Design choices and preferences besides cruise Mach number, mission range, materials technology, propulsion technology, and number of passengers also influenced the shape of the low-boom configuration of the three concepts. Some of these choices promoted low boom at the expense of high aerodynamic efficiency, while others worked in a reverse fashion and emphasized aerodynamic efficiency. The integration and blending of all these selected component features into wing-fuselage-fin-nacelle configurations produced concepts that looked very much alike, yet were very different. A short list of the three concepts' physical and mission characteristics is given in Appendix A.

Wind-Tunnel Models of Follow-on Low-Boom Concepts

The second step in the validation process involved designing and building wind-tunnel models of the three follow-on low-boom concepts. Each of the three concepts was scaled by a factor of 1:300 so that 12-inch long models could be built. Near-field pressure signatures, measured in the wind-tunnel, would be used to assess the usefulness and capabilities of the methodology as well as the merits of its application. Two sets of engine nacelles were built and used on both the LB-16 and the HSCT-10B wind-tunnel models during the measurement of their pressure signatures. One set of nacelles had low-drag features corresponding to high-performance engines, and the other set was sized for present-day-performance engines.

All three wind-tunnel models had integral fuselage/sting/balances. Two sets of strain-gages were recessed in the aft end of the stings to form a lift-pitching moment balance so that lift could be set and monitored during measurement of pressure signatures in the wind tunnel. Each model/sting/balance was about 32-inches long from nose to angle-of-attack mechanism junction. The fuselage and sting segments were long and slender enough to provide a pressure signature free of disturbances from the angle-of-attack mechanism or the wind-tunnel strut at the design Mach number, yet short enough to meet sting-divergence and local safety factor criteria.

Analysis of Pressure Signature Data From Three Low-Boom Models

The third step in the validation process was the measurement of pressure signatures generated

by the three low-boom models in the wind tunnel. In step four, these pressure signatures were analyzed and compared with expected results. As in previous wind-tunnel studies, the merits of each concept would be judged by measuring pressure signatures at two or more lift coefficients. Decreasing the wing lift, i.e. a lower $C_L / C_{L,CRUISE}$ ratio, reduced the wing-lift-induced disturbances, so the fuselage volume, wing volume, nacelle volume, and nacelle-wing interference lift disturbances could be identified more readily. This technique had been used before, e.g. references 21 and 22.

In the following sections, samples of the pressure signatures generated by wind-tunnel models of the three concepts are presented and discussed. Whitham F-functions in the reference of each concept aided in identifying the signature features, and evaluating the effectiveness of their component integration, but no theoretical signatures were presented in the following discussions.

B935 Model Pressure Signatures

Sample pressure signatures from the low-boom wind-tunnel model of the B935 concept, figure 7, are shown in figures 10 and 11.
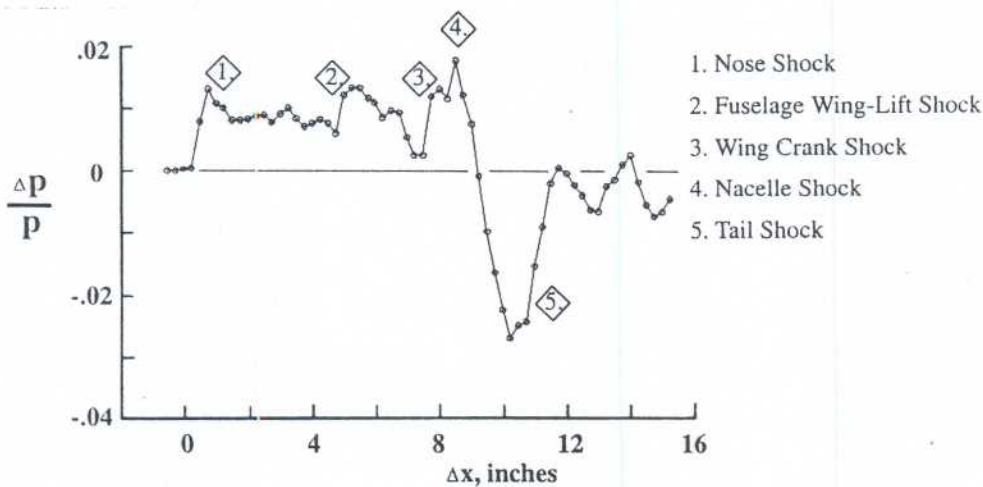

1. Nose Shock
2. Fuselage Wing-Lift Shock
3. Wing Crank Shock
4. Nacelle Shock
5. Tail Shock

Figure 10. B935 model pressure signature. M = 1.7, h = 12 inches, $C_L / C_{L,CRUISE} = 0.4$.

1. Nose Shock
2. Fuselage Wing-Lift Shock
3. Wing Crank Shock
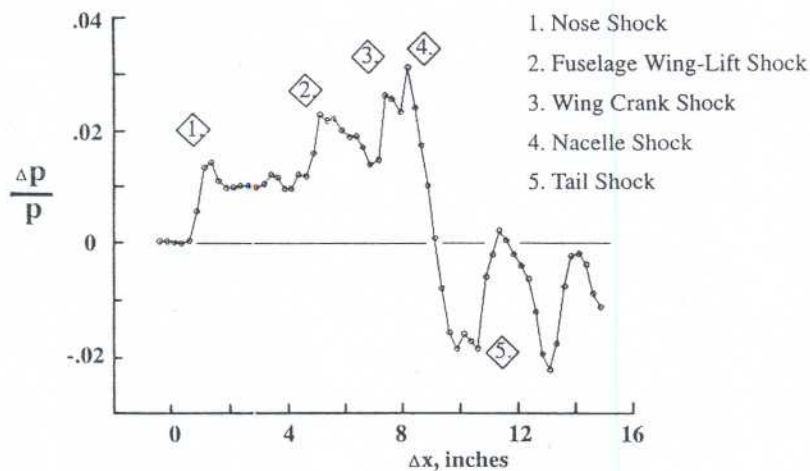4. Nacelle Shock
5. Tail Shock

Figure 11. B935 model pressure signature. M = 1.7, h = 12 inches, $C_L / C_{L,CRUISE} = 1.0$.

11

The pressure signatures in figures 10 and 11 were overlaid in figure 12 so that the differences in the two signatures would be easier to see and identify.
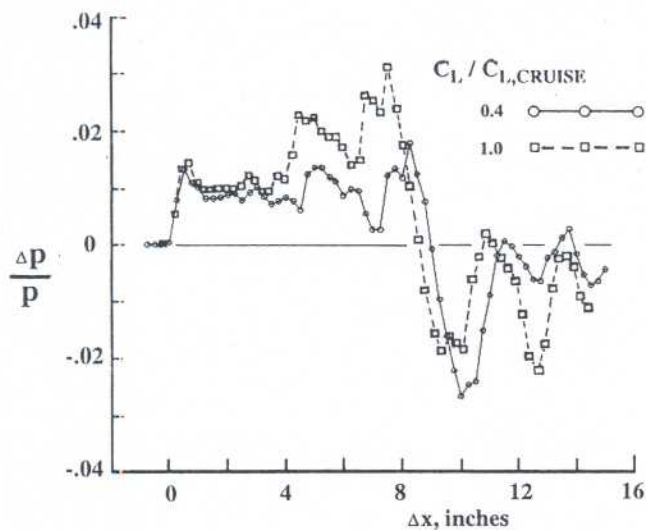

Figure 12. B935 model pressure signatures. $M = 1.7$, $h = 12$ inches, $C_L / C_{L,CRUISE} = 0.4$, and 1.0.

The nose, wing-body, leading-edge crank, and nacelle shocks are labeled as they were in reference 23. Nose, wing-body, and nacelle shocks on the pressure signature in figure 10 had about the same strength as the pressure signature in figure 11 because they were primarily volume-induced shocks, while the wing-body junction shock was caused by both volume and incremental lift discontinuities across the body/wing leading-edge junction. This wing-body junction shock had a lower strength at $C_L / C_{L,CRUISE} = 0.4$, than it did at $C_L / C_{L,CRUISE} = 1.0$, due to lower the lift gradients. Volume effects from the wing leading edge cranks, the nacelle inlet lips, and the nacelle-wing interference lift were the probable causes of the next two shocks because they were about the same in both figures 10 and 11. Several additional shocks were seen following the expansion and tail shock during the recompression to ambient pressure. These were probably due to interference between the sting and the flow off the nacelle boattail, the aft fuselage closure, and the wing downwash.

The increase in wing lift produced a very noticeable change in the shape of the two pressure signatures seen in figures 10 to 12. Unexpected shocks on both pressure signatures in figures 10 and 11 indicated the desired "ramped" low-boom shape on the positive-impulse segment of the measured pressure signature from the B935 model would not, or could not, form at the near-field distance of 12 inches. However, if an overpressure "averaging" line were used in figure 10, the top of the positive-pressure section would have a very shallow "ramped" shape. This "averaging" line technique was applied to the overpressures in figure 11 with some degree of caution because of the markedly increased wing-lift shock strength and signature impulse, I.

LB-16 Model Pressure Signatures

Like the B935 and the HSCT-10 B, this concept low-boom was tailored to generate a 1.0 psf overpressure on the ground. During the wind-tunnel tests, pressure signatures from the wind-

tunnel model of the LB-16 concept, figure 8, were measured at lift coefficient ratios similar to those on the B935 model. Like the HSCT-10 B, pressure signatures from the model with two sets of nacelles were measured. Pressure signatures, measured at lift ratios of $C_L / C_{L,CRUISE} = 0.5$ and 1.0 with the small engine nacelles on the model, are presented in figures 13 and 14.
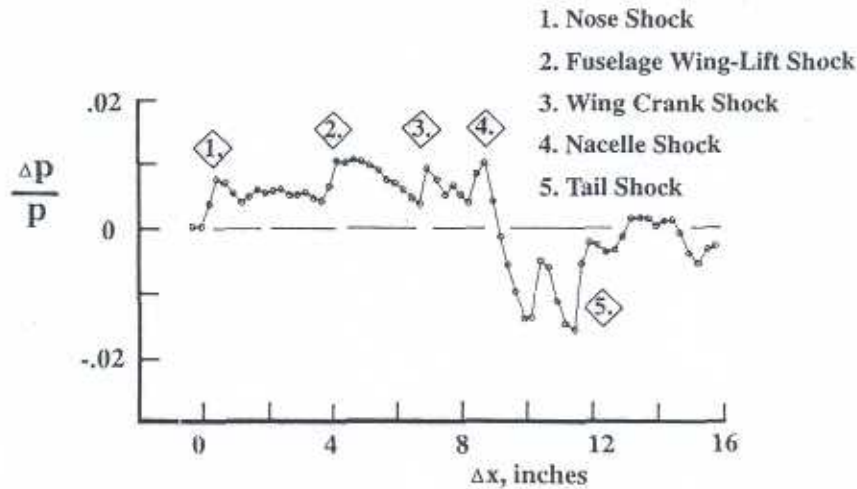

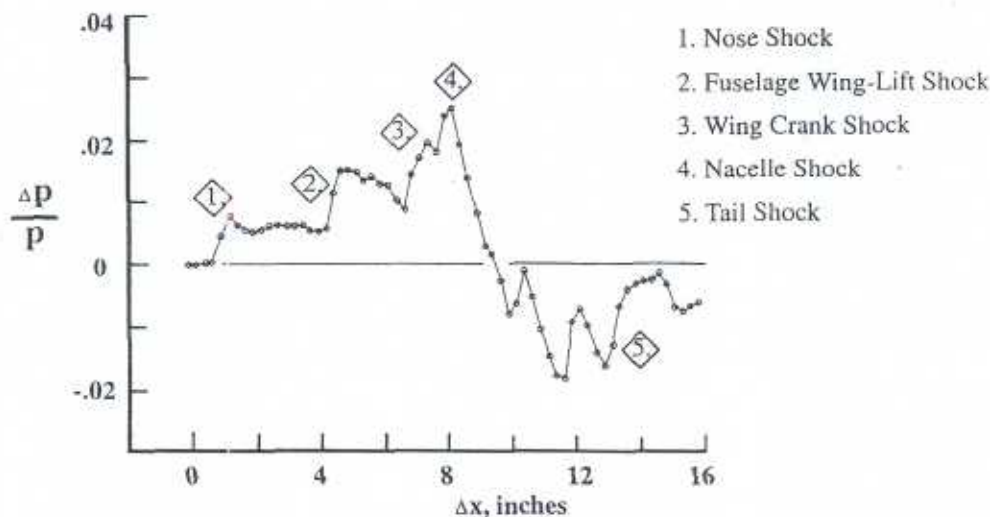Figure 13. LB-16 model pressure signature. Small engine nacelles, $M = 1.6$, $h = 20$ inches, $C_L / C_{L,CRUISE} = 0.5$.

Figure 14. LB-16 model pressure signature. Small engine nacelles, $M = 1.6$, $h = 20$ inches, $C_L / C_{L,CRUISE} = 1.0$.

As was done before with the B935 model pressure signatures, the pressure signatures shown in figures 13 and 14 are overlaid and presented in figure 15 so that the differences in the features on the two pressure signature would be easier to see and identify.
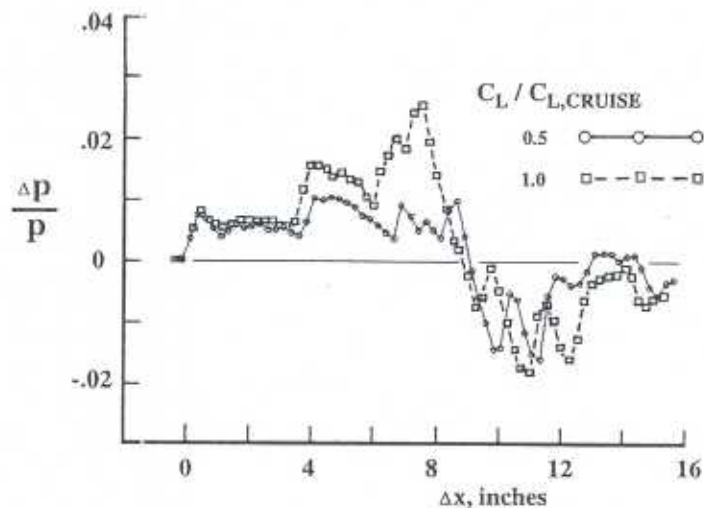
Figure 15. LB-16 model pressure signatures. Small engine nacelles, M = 1.6, h = 20 inches, $C_L / C_{L,CRUISE}$ = 0.5 and 1.0 .

Although these pressure signatures were measured at a different Mach number (1.6 rather than 1.7), and at a different separation distance (20 inches rather than 12 inches) than the pressure signatures of the B935 model, there are many similarities in the shock locations, the shock strengths, and the pressure signature shape. The second and third shocks behind the nose shock on the $C_L / C_{L,CRUISE}$ = 0.5 and $C_L / C_{L,CRUISE}$ = 1.0 pressure signatures, figures 13 and 14, have similar strengths. The third shock, due to the wing leading-edge crank, had increased considerably in strength from figure 13 to figure 14, since the lift on the model pressure signature in figure 14 was double that in the previous pressure signature, and the wing crank shock occurred where the lift gradients had probably reached their peak. Since the fourth shock had the same strength on both signatures, it was most likely due to disturbances from the nacelles. These disturbance features were seen on the B935 pressure signatures as well.

The nacelles inlets on the LB-16, like those on the B935, were longitudinally staggered, and the nacelles were mounted as far aft along the wing chord as possible. Yet, nacelle volume and interference-lift disturbances were found in the near-field pressure signatures of the LB-16 model, figures 13 to 15. Wing-body, wing leading-edge crank, and nacelle shocks, evident on both of the LB-16 pressure signatures, were not expected since the revised low-boom design and component integration methods were used. However, the LB-16 pressure signature in figure 13 did have an approximately "ramped" shape, just as the B935 pressure signature did in figure 10.

The many similarities in the measured pressure signatures from both the B935 and the LB-16 configurations (with similarly-shaped wing planforms and similar locations for nacelles) suggested that mounting engine nacelles along the under-wing trailing edges of highly-swept and modestly-notched arrow wings produced low-boom integration difficulties. Past low-boom design experience had indicated that potential low-boom benefits might be obtained by mounting nacelles on the aft fuselage of a HSCT concept. The next set of measured pressure signatures was generated by one possible aft-fuselage-nacelle concept design.

The wind-tunnel model of the HSCT-10B concept (figure 9), like the wind-tunnel model of the LB-16 concept (figure 8), was designed with two sets of engine nacelles (see Appendix B). Each set of nacelles enclosed engines that operated at different levels of propulsion technology. Pressure signatures were measured at two lift coefficients with the two sets of nacelles, and are presented in the next set of figures. These pressure signatures were generated by the model at Mach 1.8, and at a separation distance of 24 inches. The extra figures are presented to demonstrate the results of the engine nacelle location, and the similarities observed in pressure signature shapes in spite of the differences in the geometric contours of the two sets of nacelles.

Figure 16 shows a pressure signature measured with the small nacelles on the model whose attitude was set to develop a $C_L = 0.0511$, half of $C_{L,CRUISE} = 0.1022$.
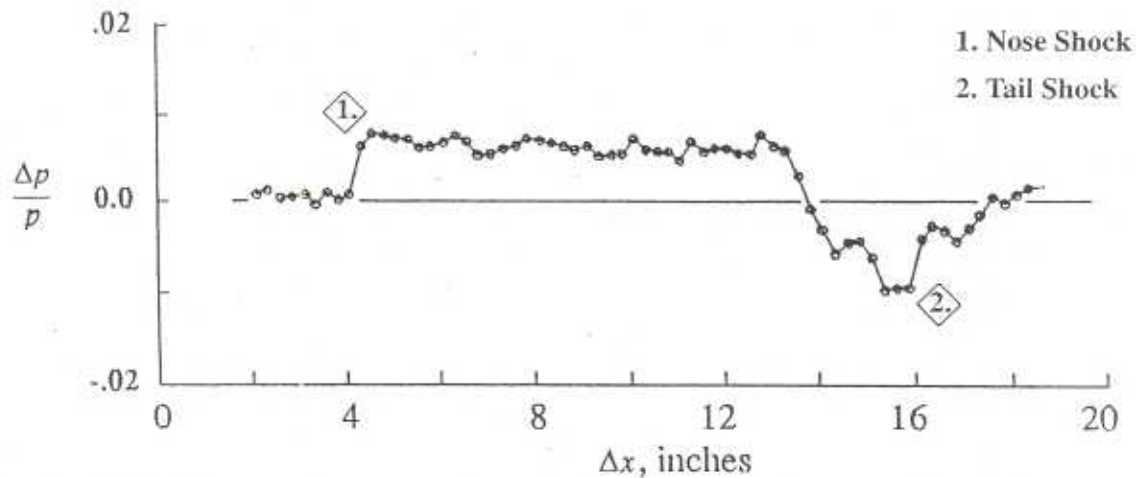

Figure 16. HSCT-10B model pressure signature. Small nacelles, M = 1.8, $C_L = 0.0511$, with $h = 24$ inches.

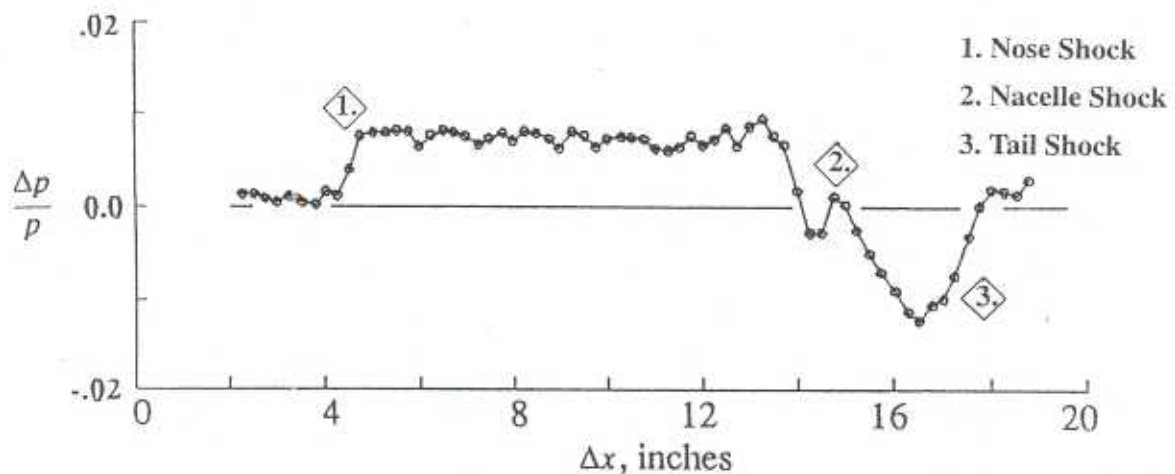The pressure signature with large nacelles on the model at a $C_L = 0.0511$ is shown in figure 17.

Figure 17. HSCT-10B model pressure signatures. Large nacelles, M = 1.8, $C_L = 0.0511$, with $h = 24$ inches.

15

The shape of the positive-pressure sections of the measured pressure signatures in figures 16 and 17 are almost identical, even though the large nacelles were about 19-percent longer and 39-percent wider than the small nacelles. Pressure signature tops were almost flat without any indication of fuselage-strake, wing-fuselage, wing leading-edge crank, or nacelle shocks. However, the C_L of the model that generated these two signatures was only half of $C_{L,CRUISE}$. When the C_L on the model was increased to 0.1022, i.e. to $C_L / C_{L,CRUISE} = 1.0$, the pressure signatures shown in figures 18 and 19 were measured.
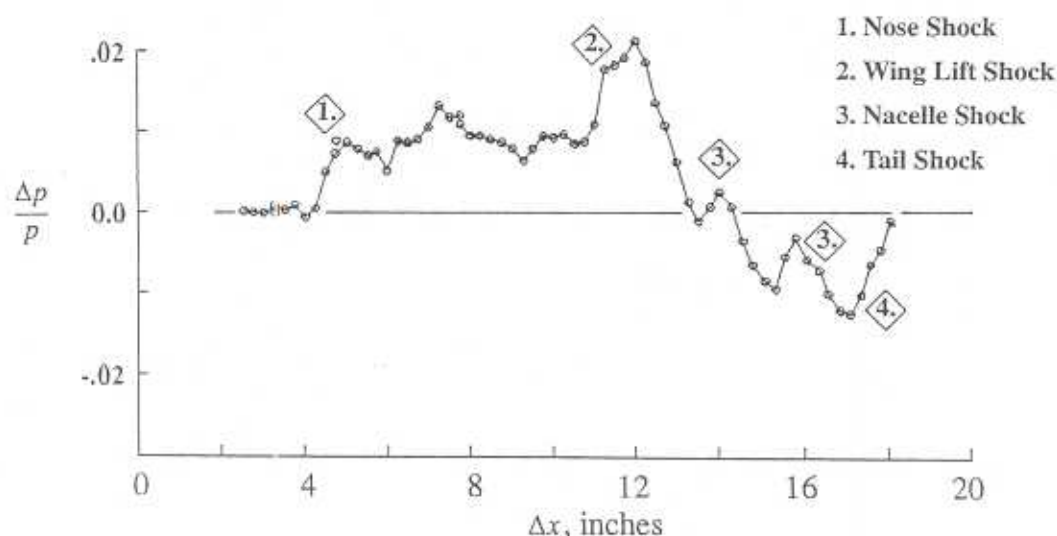

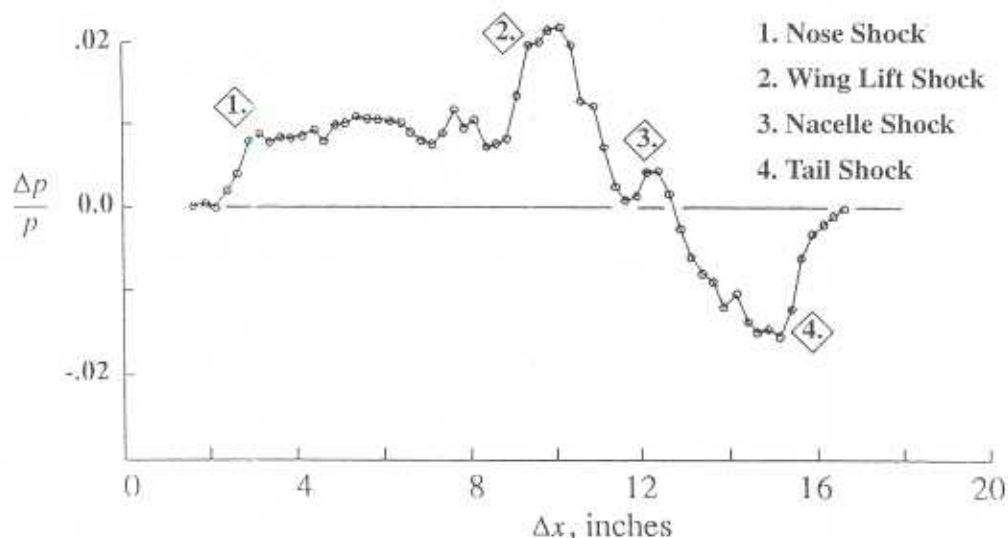Figure 18. HSCT-10B model pressure signature. Small nacelles, M = 1.8, C_L = 0.1022, with h = 24 inches.

Figure 19. HSCT-10B model pressure signature. Large nacelles, M = 1.8, C_L = 0.1022, with h = 24 inches.

Again, the positive-pressure sections of the pressure signatures, figures 18 and 19, were very

16

similar in overall shape and length. The small differences in the overpressure data following the nose shock and preceding the wing-lift shock were judged to be random data-acquisition perturbations. These disturbances come from the same components (other than nacelles) on the model with the same attitude for both of the pressure signatures (also see figures 16 and 17), and did not consistently appear on other pressure signatures recorded at the same test conditions.

The strong shocks that appear prominently before the expansion to the tail shock system in figures 18 to 19 are caused by the increase in wing lift rather than by the nacelles. As the lift ratio, $C_L/C_{L,CRUISE}$, increased from 0.50 to 1.0, the almost-flattop pressure signatures seen in figures 16 and 17 changed to the lift-shock dominated pressure signatures seen in figures 19 and 20. Since the wing leading edge, lift gradients, and volume growth on the HSCT-10B concept and model were designed to be smooth and continuous, the emergence and growth of the lift-induced shock caused concern about the applicability of the low-boom tailoring techniques employed on the concept and the wind-tunnel model.

This progressive change in pressure signature shape, for the model with large nacelles, is shown in figure 20.
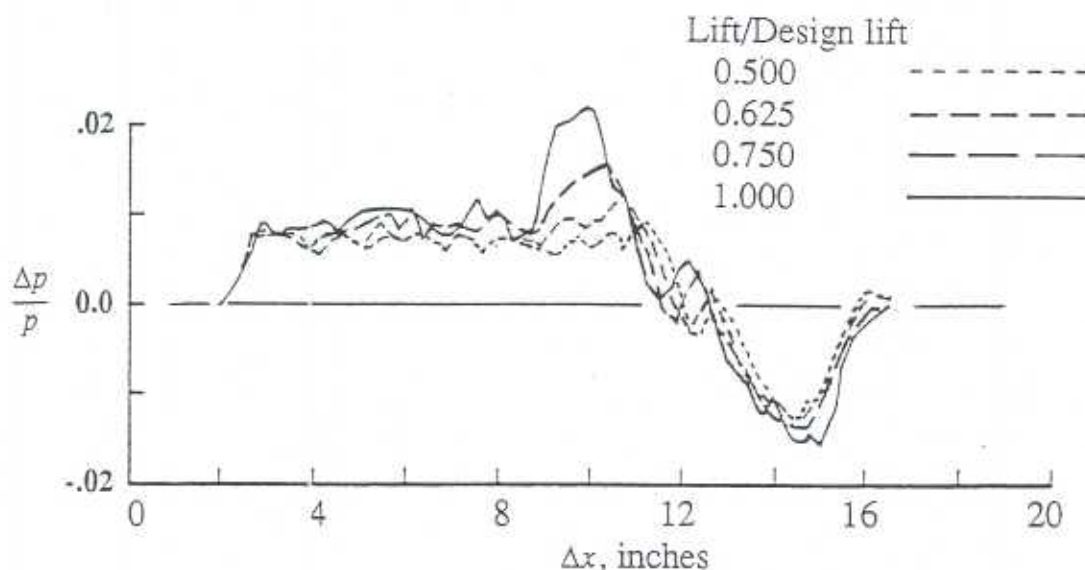

Figure 20. HSCT-10B model pressure signatures. Large nacelles, M = 1.8, h = 24 inches, with $C_L/C_{L,CRUISE}$ ratios of 0.50, 0.625, 0.75, and 1.0 .

The shock, seen in figure 20, grew during a relatively small incremental increase in angle of attack - about 1.6 degrees. It indicated there must have been a significant change in the character of the near-field flow-field disturbances due to the increase in the wing's lift. Lift gradients along the wing had supported an almost "flat-top" shape at $C_L / C_{L,CRUISE} = 0.50$, but with increasing C_L, a lift-induced overpressure perturbation grew. At $C_{L,CRUISE}$, a strong shock rather than a gradual pressure rounding marked the end of the pressure signature's mid-section ramp, and the beginning of the expansion leading to the tail shock. Similar shock behavior was also seen and noted in the pressure signatures of the Mach 2.7 low-boom, arrow-wing, sonic-boom model in figure 13(b)of reference 24.

Figure 20 demonstrated how an increasing lift gradient changed a mild isentropic compression into a strong shock over a range of about 1.6 degrees in angle of attack. Although small in

magnitude, the 1.6 degrees increase in angle of attack corresponded to an increase in equivalent area-due-to-lift from 400 ft^2 to 800ft^2. With the maximum equivalent area of the full-scale concept's volume at about 260 ft^2, the contribution of the cruise lift to the flow-field disturbances was over three times that of the volume. While the concept's volume occupied an effective length of about 300 feet, the growth of the lift, from start to finish, extended over an effective length of about 225 feet. Thus, the effective length for control of the lift, the dominant contribution to sonic boom, was less than the concept's effective length available for the control of the volume and the lift. Therefore, the need for full control of the local gradients and magnitudes in the lift distribution was demonstrated by these three HSCT concepts. It would be the key element in the successful design of a low-boom HSCT or any low-boom concept.

Discussion

Three sets of pressure signatures were the basis for judging the capabilities and applicability of some revised sonic-boom analysis methods, low-boom design tools, and engine-nacelle integration techniques. These pressure signatures, generated by three wind-tunnel models, were measured at different separation distances and different Mach numbers.

When the separation distances corresponding to these measured pressure signatures were made non-dimensional by the model's span, interesting and encouraging trends seemed to emerge. In the B935 model pressure signatures, figures 10 through 12, the separation distance ratio, h/b, was 2.14; in the LB16 model pressure signatures, figures 13 through 15, h/b was 3.57; and in the HSCT-10B model pressure signatures, figures 17 through 21, h/b was 4.0. At each h/b separation, the B935 and LB-16 pressure signatures shapes were perturbed with low-intensity and high-intensity shocks. This same behavior was noted in the near-field pressure signatures of both the Mach 2 and the Mach 3 wind-tunnel models, figures 5 and 6.

In spite of the shocks along the positive section of some of the pressure signatures that interrupted a smooth build-up of overpressure, an "averaging line" smoothing of these overpressures suggested that a "ramped" signature shape might be developing. This suggestion was based on a near-field, localized-flow model of pressure signature shape behavior that predicted the between-shock pressure perturbations and the observed lift-induced shocks would decrease in strength with increasing separation distance, well before they could coalesce with the nose shock. As the shocks decreased in strength, the "ramp" section of the signature would lose its "roller-coaster" appearance and approach the shape of the desired ground signature. This seemed to be an optimistic conclusion although similar trends were seen in figures 2 through 5 in reference 25, or figures 3 to 5 in reference 26.

The near-field lift-induced shocks seen in the HSCT-10B measured pressure signatures were less numerous and less complex than the measured pressure signatures from the B935 and the LB-16 models. Perhaps it was because both the B935 and the LB-16 models had engine nacelles mounted under the wings, while the HSCT-10B had engine nacelles on the aft fuselage behind the wing trailing edge. The smooth and continuous curved leading edge on the HSCT-10B wing versus the segmented straight-line leading edges on the B935 and LB-16 wings may also have contributed to the less-complex pressure signatures. Whatever the cause or causes, it is apparent that in the less "cluttered" HSCT-10B model's pressure signatures, the disturbance effects were easier to see and the pressure signature features were less difficult to interpret.

Although the three concepts had about the same overall length, wing span, and aspect ratio,

the equivalent areas due to lift (listed in Appendix A) and wing loading at start of cruise were noticeably different. Additional shocks in the pressure signatures of the B935 and the LB-16 were, therefore, the result of geometry choices during the concepts' design. Their strengths and positions along the pressure signature might, under unfavorable atmospheric conditions, might force these shocks to coalesce with the nose shock as the separation distance increased, but there seemed to be some trends toward smooth signature-top "ramping". This last conclusion is optimistic but conjectural, since the issue cannot be firmly settled with the existing wind-tunnel data. Further wind-tunnel tests would be needed for verification.

The HSCT-10B wind-tunnel model pressure signatures presented in figures 17 through 21 validated the conclusion that properly-contoured engine nacelles could be successfully integrated onto the wing/fuselage of a conceptual aircraft, and that the revised nacelle-integration methodology could predict the nacelle-volume disturbances with reasonable accuracy. From this optimistic point of view, it is also probable that the revised nacelle-integration method could predict nacelle-wing interference lift with sufficient accuracy to make this multiple-use tool fully useful for preliminary conceptual design.

Nacelle-wing interference-lift is very important to the performance of a configuration with engine nacelles mounted under the wings. The results of this test were not favorable toward recommending this engine-nacelle location, but did not negate the feasibility of mounting nacelles under the wing as a possible design choice. More tests of low-boom concepts and their corresponding wind-tunnel models having the nacelles in this location would be required before this conclusion and judgement could be made with absolute certainty.

Concluding Remarks

Pressure signatures measured in wind-tunnel tests of two low-boom models demonstrated that the methods developed prior to the late 1970's needed to be revised. With the revisions in place, they could be used to analyze an aircraft's sonic-boom characteristics accurately, and to integrate the aircraft components on supersonic-cruise conceptual aircraft for favorable low-boom characteristics. The validity and applicability of the revised design, analysis, and integration methods were assessed by employing them to design three follow-on low-boom conceptual aircraft. Wind-tunnel models of these concepts were built, and used to measure pressure signatures in the wind tunnel.

An analysis of the measured pressure signatures showed both favorable and unfavorable results. Wing-integration and nacelle-integration disturbances were found on the pressure signatures from both of the nacelle-under-the-wing wind-tunnel models. This strongly suggested that design compromises to achieve high lift / drag ratio mission performance and low-boom characteristics with a wing-fuselage-fin configuration might be extremely difficult with nacelles mounted conventionally under the configuration's wing. Pressure signatures from the model with the nacelles located on the aft fuselage behind the wing, the HSCT-10B, indicated that the desired low-boom integration of nacelles with the wing-fuselage-fin had been achieved with both small, high-technology engine nacelles and with larger, "realistic"-technology, nacelles. This result demonstrated the applicability of the revised design and nacelle-integration methodology, insofar as nacelle-volume-alone effects were concerned. It was concluded that satisfactorily predictions of nacelle-wing interference lift effects might be obtained with the revised design and analysis methods, but additional wind-tunnel models and pressure-signature-measurement tests would be

necessary to confirm this expectation of favorable results.

In addition to these nacelle-integration results, unexpected near-field lift-induced shocks were found on the pressure signatures from all three models. It was concluded that these shocks could be due to both the model geometry, and to the physical characteristics of the flow at the near-field distances where the models' pressure signatures were measured. They were hypothesized to be near-field-enhanced disturbances that would attenuate and disappear with increasing distance. If this hypothesis was correct, the nose shock would have only the low-boom-designed strength on the ground. At the separation distances available in the wind-tunnel test section, this hypothesis could not be tested.

In all three conceptual aircraft designs, high aerodynamic efficiency and low-boom technology features were incorporated into the configurations at the expense of low-structural weight. If the results of this study were the basis for new conceptual designs, more effort would needed in reducing the empty weight by modifying the leading-edge sweep, and by reducing the trailing-edge "notching," in an effort to make the aft-wing spar as straight and normal to the aircraft center line as possible. If the engine nacelles were mounted under the wings to attain high aerodynamic efficiency, they would have to be carefully integrated into the configuration to keep the nacelle disturbances from coalescing with, and possibly adding strength to, the nose shock.

These three concepts were methodology validation concepts, very similar to the Mach 2 and Mach 3 validation concepts that preceeded them. The wing/fuselage/nacelle/fin geometries applied to their configurations addressed the difficulties in designing conceptual aircraft that had high aerodynamic efficiency, optimistic engine performance, low-boom component features, and low structural weight. Some were shown to be inadequate while others were only partially successful. All were employed for reasons that seemed sound at the time. In this regard, they served their purpose well.

References

1. Taylor, John W. R., ed.: *Jane's All The World Aircraft*, 1967-68, 58th Edition. pp. 320-321, McGraw-Hill Book Company, New York, USA. (North American XB-70)

2. Taylor, John W. R., ed.: *Jane's All The World Aircraft*, 1967-68, 58th Edition. pp. 87-88, McGraw-Hill Book Company, New York, USA. (British-French Concorde)

3. Gunston, Bill: Aircraft Of The Soviet Union. pp. 345-349, Osprey Publishing Limited, 1983. (Tupelov Tu-144D)

4. Taylor, John W. R., ed.: *Jane's All The World Aircraft*, 1969-70, 60th Edition. pp. 282-283, McGraw-Hill Book Company, New York, USA. (Boeing 2707-300)

5. Taylor, John W. R., ed.: *Jane's All The World Aircraft*, 1969-70, 57th Edition. pp. 274, McGraw-Hill Book Company, New York, USA. (Lockheed Model 2000)

6. Morris, Odel A.; and Fournier, Roger H.: *Aerodynamic Characteristics At Mach Numbers 2.30, 2.60, and 2.96 Of A Supersonic Transport Model Having A Fixed, Warped Wing.* NASA TM X-1115, 1965. (Supersonic Cruise Aircraft Transport SCAT-15F)

7. Baber, Hal T.; and Swanson, E. E.: *Advanced Supersonic Technology Concept AST-100*

Characteristics Developed In A Baseline-Update Study. NASA TM X-72815, January, 1976.

8. Fitzsimmons, R. D.; and Roensch, R. L.: *Advanced Supersonic Transport.* Society of Automotive Engineers, Air Transport Meeting, May 6-8, 1975. (MDC-AST)

9. Robins, A. Warner; Dollyhigh, Samuel M.; Biessner, Fred L.; Geiselhart, Karl; Martin, Glenn L.; Shields, E. W.; Swanson, E. E.; Coen, Peter G.; and Morris, Shelby J.: *Concept Development Of A Mach 3.0 High-Speed Civil Transport.* NASA TM 4058, 1988.

10. Domack, Christopher S.; Dollyhigh, Samuel M.; Biessner, Fred L.; Geiselhart, Karl; McGraw, Marvin E.; Shields, Elwood E.; and Swanson, Edward E.: *Concept Development Of A Mach 4.0 High-Speed Civil Transport.* NASA TM 4223, 1990.

11. Mack, R.; and Needleman, K.: *The Design Of Two Sonic-Boom Wind-Tunnel Models From Conceptual Aircraft Which Cruise At Mach Numbers Of 2.0 and 3.0.* AIAA-90-4026, 13th AIAA Aeroacoustics Conference, Tallahassee Florida, October 22-24, 1990.

12. Mack, Robert J.; and Needleman, Kathy E.: *A Methodology For Designing Aircraft To Low Sonic Boom Constraints.* NASA TM 4246, February 1991.

13. Mack, Robert J.; and Needleman, Kathy E.: *A Semiempirical Method For Obtaining Fuselage Normal Areas From Mach-Sliced Areas.* NASA TM 4228, December 1990.

14. Whitham, G. B.: *The Flow Pattern of a Supersonic Projectile.* Communications on Pure and Applied Mathematics vol. V, no. 3, August 1952, pp. 301-348.

15. Mack, Robert J.: *Some Considerations On The Integration Of Engine Nacelles Into Low-Boom Aircraft Concepts.* High-Speed Research: Sonic Boom, Volume II, NASA Conference Publication 3173, 1992.

16. McCullers, L. A.: *Aircraft Configuration Optimization Including Optimized Flight Profiles. Recent Experiences In Multidisciplinary Analysis And Optimization.* Jaroslaw Sobieski, compiler, NASA CP-2327, Part 1, 1984.

17. Thomas, Charles L.: *Extrapolation Of Sonic Boom Pressure Signatures By The Waveform Parameter Method.* NASA TN D-6832, 1972.

18. Haglund, George T.: *Low Sonic Boom Studies At Boeing.* High-Speed Research: Sonic Boom, Volume II, NASA Conference Publication 10133, 1993.

19. Baize, Daniel G.; and Coen, Peter G.: *A Mach 2.0 / 1.6 Low Sonic Boom High-Speed Civil Transport Concept.* High-Speed Research: Sonic Boom, Volume II, NASA Conference Publication 10133, 1993.

20. Mack, Robert J.: *Low-Boom Aircraft Concept With Aft-Fuselage-Mounted Engine Nacelles.* High-Speed Research: Sonic Boom, Volume II, NASA Conference Publication 10133, 1993.

21. Carlson, Harry W.; McLean, F. Edward; and Shrout, Barrett L.: *A Wind-Tunnel Study Of Sonic-Boom Characteristics For Basic And Modified Models Of A Supersonic Transport Configuration.* NASA TM X-1236, May 1966.

22. Hunton, Lynn W.; Hicks, Raymond M.; and Mendoza, Joel P.: *Some Effects Of Wing*

Planform On Sonic Boom. NASA TN D-7160, January 1973.

23. Haglund, George T.: *Boeing HSCT Concepts For Low Sonic Boom: Design, Analysis, And Wind Tunnel Test*. Boeing Document No. D6-81804, Boeing Aircraft Company, 1996.

24. Mack, Robert J.; and Darden, Christine M.: *Wind-Tunnel Investigation Of The Validity Of A Sonic-Boom-Minimization Concept*. NASA TP 1421, October 1979.

25. Mack, Robert J.: *Persistence Characteristics In Wind-Tunnel Pressure Signatures From Two Similar Models*. NASA / TM-2004-212671, January 2004

26. Mack, Robert J.: *An Analysis Of Measured Pressure Signatures From Two Theory-Validation Low-Boom Models*. NASA / TM-2003-212423, October 2003

27. Mack, Robert J.; and Haglund, George T.: *A Practical Low-Boom Overpressure Signature Based On Minimum Sonic Boom Theory*. High-Speed Research: Sonic Boom, Volume II, NASA Conference Publication 3173, February 1992.

Appendix A

Sample Design And Mission Data From The Three Follow-On Low-Boom Concepts.

Mission Description

	B935	LB-16	HSCT-10B
Low-Boom Mach Number	1.7	1.6	1.8
Low-Boom Ground Overpressure, psf	1.0	1.0	1.0
Over-Water Mach Number	2.4	2.0	2.4
Mission Range, nmi	5,000	6,500	5,000
Number of Passengers	300	250	300
Shape Of Low Boom Pressure Signature	"Hybrid"**	"Ramp"	"Hybrid"**

Configuration Description

	B935	LB-16	HSCT-10B
Wing Area, S, ft^2	9,000	9,263	10,465
Wing Span, b, ft	140	140	150
Aspect Ratio, b^2/S	2.18	2.12	2.15
Length, ft	317	295	328
A_E, Lift, Start of Cruise, ft^2	680.4	778.5	800.5
$C_{L,CRUISE}$ at Low-Boom Mach Number	0.11742	0.13458	0.10335

Configuration Weights

	B935	LB-16	HSCT-10B
Gross Takeoff Weight, W_{GTO}, lb	731,600	646,356	662,000
Beginning Cruise Weight, W_{BC}, lb	694,000	609,000	618,000
W_{BC}/S, lb/ft^2	77.1	65.7	59.1
Empty Weight, W_E, lb	319,300	203,310	246,000
W_{GTO}/W_E	2.29	3.18	2.69

** The "Hybrid" signature is a "Ramped" signature with a short "Flat-top" section between the nose shock and the onset of the isentropic pressure-rise "Ramp". See reference 27 for description and discussion of the "Hybrid" pressure signature.

Appendix B

HSCT-10B Concept Engine Nacelles.

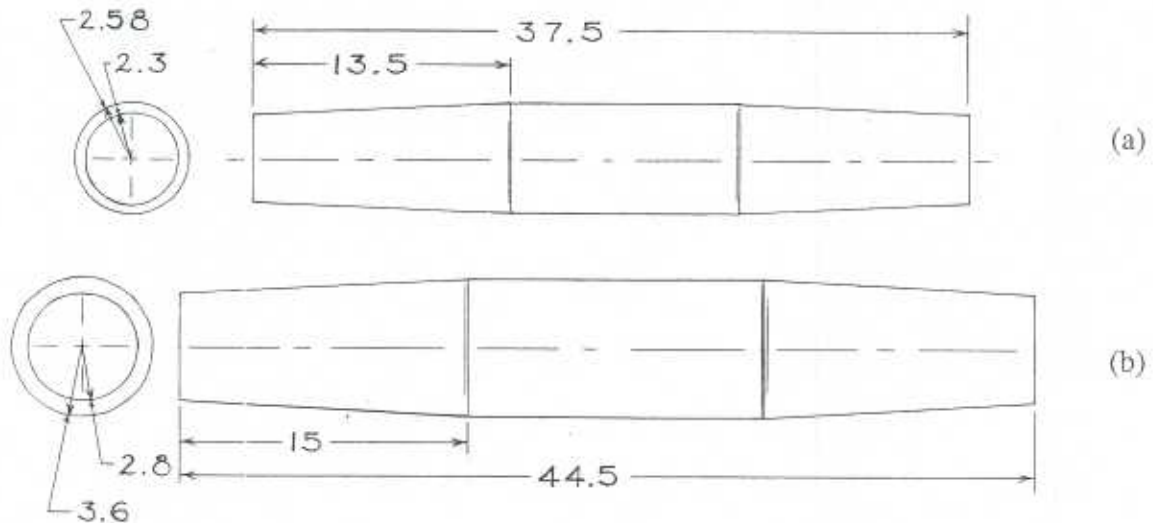The engine nacelles shown in figure B1 were designed for the HSCT-10B concept.

Figure B1. Sketches of the HSCT-10B engine nacelles. All dimensions are in feet.
(a) High-performance engine, low-drag nacelle
(b) Conservative technology engine and nacelle

These nacelles were held by struts mounted on the aft fuselage of the HSCT-10B. Both of the nacelles were far enough behind the wing trailing edge to assure no nacelle disturbances would impinge on the wing's upper surface during cruise. The struts had dihedral to increase the effective distance between each nacelle and the nose. They were made high enough to keep the inlet of the inside nacelle above the fuselage's boundary layer displacement thickness, yet as short as possible to minimize the effect of engine-out yaw.

REPORT DOCUMENTATION PAGE

Form Approved
OMB No. 0704-0188

1. REPORT DATE *(DD-MM-YYYY)*	2. REPORT TYPE	3. DATES COVERED *(From - To)*
01- 12 - 2005	Technical Memorandum	

4. TITLE AND SUBTITLE

An Evaluation of Measured Pressure Signatures From Wind-Tunnel Models of Three Low-Boom Concepts

5a. CONTRACT NUMBER

5b. GRANT NUMBER

5c. PROGRAM ELEMENT NUMBER

6. AUTHOR(S)

Mack, Robert J.

5d. PROJECT NUMBER

5e. TASK NUMBER

5f. WORK UNIT NUMBER

984754.02.07.07

7. PERFORMING ORGANIZATION NAME(S) AND ADDRESS(ES)

NASA Langley Research Center
Hampton, VA 23681-2199

8. PERFORMING ORGANIZATION REPORT NUMBER

L-19127

9. SPONSORING/MONITORING AGENCY NAME(S) AND ADDRESS(ES)

National Aeronautics and Space Administration
Washington, DC 20546-0001

10. SPONSOR/MONITOR'S ACRONYM(S)

NASA

11. SPONSOR/MONITOR'S REPORT NUMBER(S)

NASA/TM-2005-213927

12. DISTRIBUTION/AVAILABILITY STATEMENT

Unclassified - Unlimited
Subject Category 71
Availability: NASA CASI (301) 621-0390

13. SUPPLEMENTARY NOTES

An electronic version can be found at http://ntrs.nasa.gov

14. ABSTRACT

Revised 1990-1991 sonic-boom design and analysis methodology was assessed by applying it to the design of three low-boom concepts. Models of these concepts were built and used to measure pressure signatures in the wind tunnel. An analysis of wind-tunnel data showed unexpected nacelle-inlet and the nacelle-wing interference-lift shocks in the pressure signatures from the two engine-under-the-wing models, but not in the measured pressure signatures from the wind-tunnel model with the engine nacelles mounted on the aft fuselage. However, additional lift-induced shocks were found in the pressure signature data from all three wind-tunnel models indicating that other flow-field disturbance effects were present.

15. SUBJECT TERMS

Sonic boom; Low-boom concepts; Wind-tunnel models; Method validation

16. SECURITY CLASSIFICATION OF:			17. LIMITATION OF ABSTRACT	18. NUMBER OF PAGES	19a. NAME OF RESPONSIBLE PERSON
a. REPORT	b. ABSTRACT	c. THIS PAGE			STI Help Desk (email: help@sti.nasa.gov)
U	U	U	UU	29	19b. TELEPHONE NUMBER *(Include area code)* (301) 621-0390

Standard Form 298 (Rev. 8-98)
Prescribed by ANSI Std. Z39.18